HIGH-EFFICIENCY AMORPHOUS SILICON ALLOY BASED SOLAR CELLS AND MODULES

Quarterly Technical Progress Report
June 1, 2004 through August 31, 2004

S. Guha and J. Yang
United Solar Ovonic Corporation
Troy, Michigan

NREL Technical Monitor: Bolko von Roedern

Prepared under Subcontract No. ZDJ-2-30630-19

Overview

This report covers the work from June 1 to August 31, 2004, at United Solar Ovonic Corporation. In this quarter, we have worked in the following areas:

1. Continue to optimize nc-Si:H cells as a bottom cell to search for highest efficiency using multi-junction structures. As reported in the Phase II annual report, we have achieved an initial active-area efficiency of 14.6% using an a-Si:H/a-SiGe:H/nc-Si:H triple-junction structure. This cell has been degraded under 100 mW/cm^2 of white light at 50 ºC for over 1000 hours. The active-area stable efficiency is 12.6%, which is equivalent to 11.7% total-area stable efficiency.

2. For high rate deposition, we continued our work using MVHF glow discharge and achieved an initial active-area efficiency of 13.8% using an a-Si:H/a-SiGe:H/nc-Si:H triple-junction structure.

3. For the large-area deposition, we optimized the a-SiGe:H middle and bottom cells under the constraints of the production machine. The component cell performance has been improved.

4. We have detected powder formation during MVHF plasma deposition of a-Si:H and a-SiGe:H alloy and correlated the plasma properties to cell performance.

5. We have continued to study the metastability of nc-Si:H solar cells. We found that a forward current-injection does not degrade the nc-Si:H cell performance. Reverse electrical bias enhances light-induced degradation in nc-Si:H solar cells. These results are contrary to observations in a-Si:H solar cells. We explain these new results based on heterogeneity of the material structure.

1. High efficiency a-Si:H/a-SiGe:H/nc-Si:H triple-junction solar cells

Using the hydrogen dilution profiling technique, we have improved the nc-Si:H solar cells and achieved an initial active-area efficiency of 8.37%. Incorporating the improved nc-Si:H cell in an a-Si:H/a-SiGe:H/nc-Si:H triple-junction structure, we have obtained an initial active-area efficiency of 14.59%, which ties the record of the initial efficiency achieved using the a-Si:H/a-SiGe:H/a-SiGe:H triple-junction structure. In this quarter, we finished the stability experiment on the high efficiency a-Si:H/a-SiGe:H/nc-Si:H triple-junction solar cells. The standard light soaking condition has been used with 100 mW/cm^2 of white light at 50 ºC for more than 1000 hours.

Table I lists initial and stable J-V characteristics of a series of a-Si:H/a-SiGe:H/nc-Si:H triple-junction solar cells. The highest stable efficiency was 12.59% from Line 14863. This cell degraded by 13.5%, which is mainly from the reduction of FF. Figure 1 shows the J-V characteristics of the cell with the highest stable efficiency. From the QE spectra, one can see that the bottom cell response does not change after the light soaking, but the top cell and middle cell degraded. Overall, the stable efficiency is not better than the best stable efficiency of 13% achieved using an a-Si:H/a-SiGe:H/a-SiGe:H triple-junction cell. Although the nc-Si:H bottom cell does not degrade very much, the thicker a-Si:H top cell and a-SiGe:H middle cell might have caused the high overall degradation.

Table I: Stability of a-Si:H/a-SiGe:H/nc-Si:H triple-junction solar cells made using RF glow discharge at low rate. The underlined QE data indicate the limiting current densities.

Sample	State	Eff (%)	J_{sc} (mA/cm^2)	V_{oc} (V)	FF	QE (mA/cm^2)		
						T	M	B
14863	Initial	14.55	8.52	2.190	0.780	8.72	9.37	<u>8.52</u>
	Stable	12.59	8.33	2.128	0.710	<u>8.33</u>	8.98	8.43
	Deg.	13.5%	2.2%	2.8%	9.0%	4.5%	4.2%	1.1%
14866	Initial	14.59	8.76	2.184	0.762	8.85	9.21	<u>8.76</u>
	Stable	12.35	8.40	2.125	0.692	<u>8.40</u>	8.76	8.68
	Deg.	15.4%	4.2%	2.7%	10.0%	4.2%	4.9%	0.9%
14876	Initial	12.32	7.29	2.136	0.791	8.56	8.62	<u>7.29</u>
	Stable	11.20	7.12	2.136	0.737	8.38	8.11	<u>7.12</u>
	Deg.	9.1%	2.3%	0%	6.8%	2.1%	5.9%	2.3%
14877	Initial	13.93	8.33	2.194	0.762	8.91	8.81	<u>8.33</u>
	Stable	12.44	8.28	2.141	0.702	8.59	8.39	<u>8.28</u>
	Deg.	10.7%	0.6%	2.4%	7.9%	3.4%	4.6%	0.6%

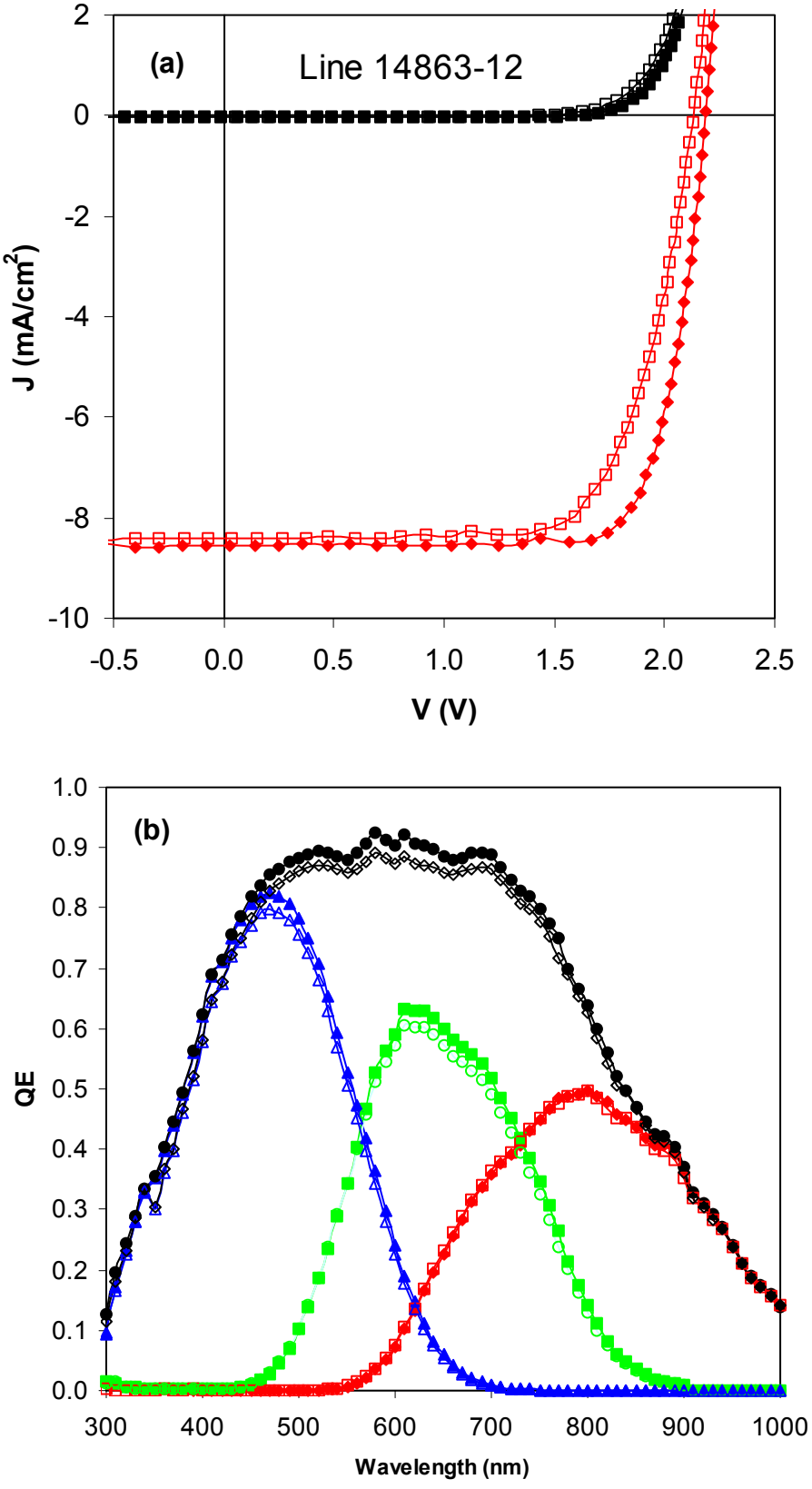

Figure 1. (a) J-V characteristics and (b) quantum efficiency of an a-Si:H/a-SiGe:H/nc-Si:H triple-junction cell at the initial (solid symbols) and stable (open symbols) states.

2. MVHF glow discharge at high deposition rate

In the Phase II annual report, we have presented an initial active-area efficiency of 12.8% in an a-Si:H/a-SiGe:H/nc-Si:H triple-junction solar cell, where the nc-Si:H bottom cell intrinsic layer was deposited by modified very high frequency (MVHF) glow discharge at high deposition rates. The corresponding parameters are J_{sc}=7.5 mA/cm^2, V_{oc}=2.159 V, and FF=0.791. The low current from the nc-Si:H bottom cell limited further improvement in the triple-junction cell efficiency. As we addressed in the previous report, the nc-Si:H film growth is subjected to microstructure evolution. By increasing film thickness, the nanocrystalline volume fraction (f_c) and grain size increase. A high f_c with large grain size causes poor grain boundary passivation and high microvoid density, which result in a poor collection for the photo-generated carriers and low current density. For the nc-Si:H cells made by MVHF using a constant hydrogen dilution ratio, a current density up to 22.5~23.0 mA/cm^2 can be obtained at a thickness of ~1.2 μm. Further increasing the thickness did not increase, but reduced the current density.

To overcome this problem, we have developed a hydrogen dilution profiling technique, where the hydrogen dilution ratio was decreased with increasing thickness. By varying the hydrogen dilution in the gas mixture during deposition, microstructure evolution has been controlled and the cell performance has been significantly improved. A 14.59% initial and 12.59% stable active-area cell efficiencies have been achieved using an a-Si:H/a-SiGe:H/nc-Si:H triple-junction solar cell made with RF glow discharge at a low rate. Lately, we have transferred this technique to MVHF at high rates. By using this technique, we are able to make thicker nc-Si:H films by increasing the power during the same deposition time while retaining good material quality. As a result, a record efficiency of 13.8% has been achieved in a triple-junction structure. Figure 2 shows (a) the J-V characteristics and (b) quantum efficiency of this cell. The deposition time for the bottom cell intrinsic layer was 60 minutes. The J_{sc} is 8.08 mA/cm^2, in contrast to J_{sc} of 7.5 mA/cm^2 in the previous champion cell. A total current of ~ 24.5 mA/cm^2 from QE measurement is much higher than that in the cell with a constant hydrogen dilution ratio in the bottom cell. The cell has a bottom cell limited current and a high FF of 0.786, indicative of a high quality nc-Si:H material. . We believe that these improvements mainly benefited from the hydrogen dilution profiling technique used in the bottom cell intrinsic layer deposition. Light-soaking experiment for this cell is under way.

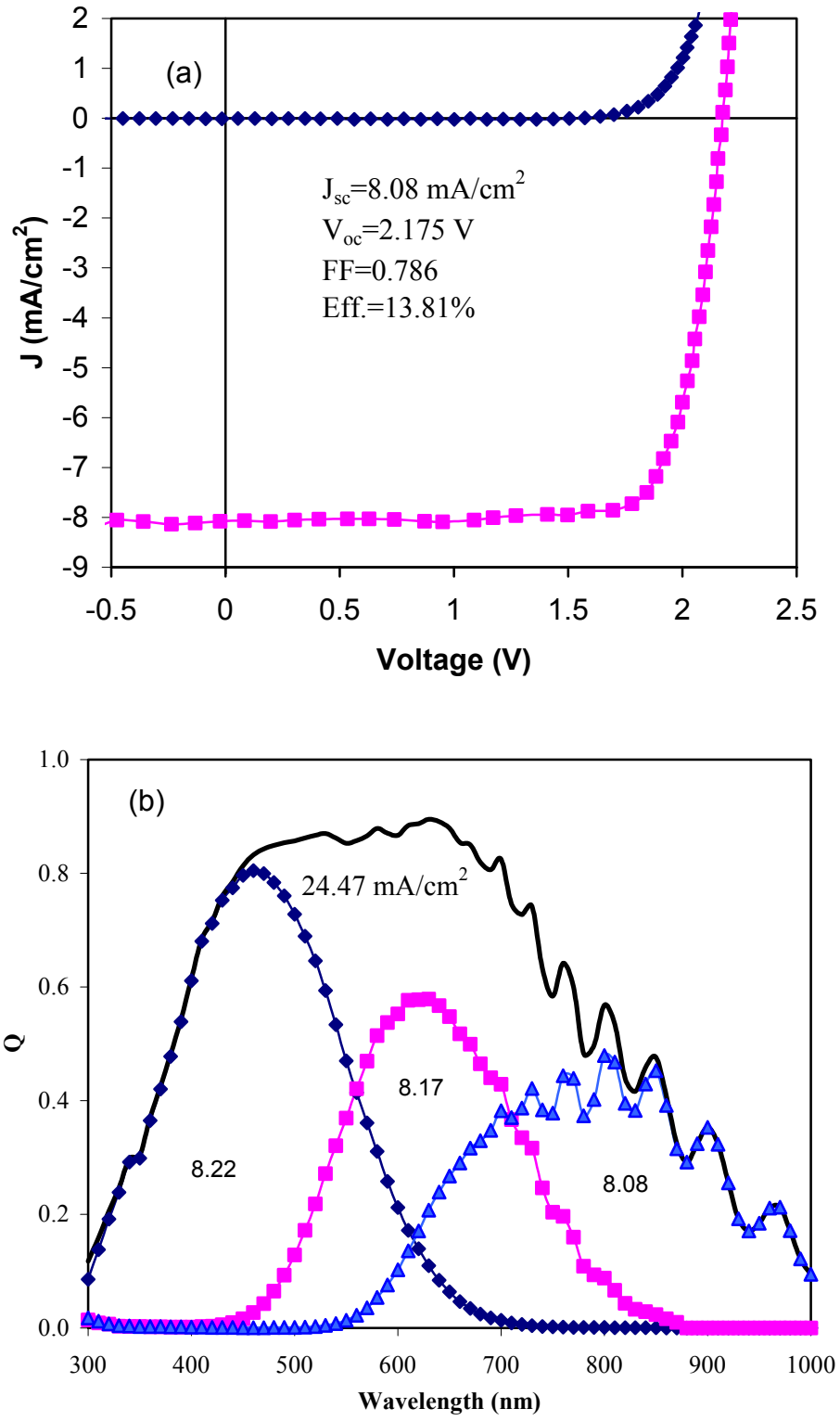

Figure 2. (a) J-V characteristics and (b) quantum efficiency of an a-Si:H/a-SiGe:H/nc-Si:H triple-junction solar cell, where the bottom cell was made using MVHF at high rate and the top and middle cells used RF at low rate.

3. Large-area deposition under the production constraints on the R&D reactor (2B)

We have continued to improve the performance of the a-SiGe:H middle cell on stainless steel and the a-SiGe:H bottom cell on Al/ZnO back reflector obtained from the production line. The deposition times for all layers were kept the same as on the production machine so that the process could be transferred relatively quickly. By systematic improvement of the layers comprising the intrinsic layer on the component cells, we have been able to obtain higher output on 0.25 cm^2 devices as shown in Table II

We note that the improvements are primarily in the fill factor, which we believe is due to the re-optimized germanium profiling for the material obtained at the higher deposition rates used in production as compared to the best a-SiGe:H alloys obtained at lower deposition rates. We are now in the process of light soaking these cells as well as making current balanced triple-junction cells and modules using these optimized component cells.

Table II: The previous best and current best active area performance on 0.25 cm^2 middle and bottom a-SiGe:H cells on stainless steel and Al/ZnO back reflectors, respectively. The middle cells were measured under AM1.5 solar simulator with a 530-nm cut-on filter, the bottom cells with a 630-nm cut-on filter.

Cell	Subst.	Spectrum	Sample	V_{oc} (V)	FF	J_{sc} QE (mA/cm^2)	P_{max} (mW/cm^2)
Previous best							
Middle	SS	>530	8316	0.704	0.666	7.85	3.7
Bottom	Al/ZnO	>630	8358	0.588	0.626	8.45	3.1
Current best performance							
Middle	SS	>530	10046	0.685	0.704	8.30	4.00
Bottom	Al/ZnO	>630	10058	0.598	0.649	8.29	3.22

4. Effect of temperature and gas flow on powder formation in high deposition rate silane, germane, and mixed gas plasmas

4.1. Introduction

The stability of a-Si:H and a-SiGe:H alloys, deposited at higher rates, is expected to depend on the formation of higher silane molecules (Si_nH_{2n+2}) in the plasma. These molecules are believed to grow into powder ($[SiH_2]_n$) when the value of n exceeds some number. We have used a non-invasive technique to track the density of powder particulates in the plasma during the deposition of a film at higher rates. We expect to learn about the evolution of the particulates in a deposition system that fabricates high efficiency solar cells at high rates (MVHF). We have looked particularly at the effects of changing the flow rate, temperature, and the addition of germane to silane, all of which are expected to have small effects on the deposition rate (compared to the power or the pressure).

4.2. Experimental

We have measured the scattered light intensity at 90° from an Ar laser (419nm) incident to the space between the cathode and substrate in a MVHF deposition system. A schematic of the arrangement is shown in Fig. 3. We have looked at the formation of powder in the plasma under various conditions. A typical spectrum is shown in Fig. 4. We define the additional scattering at the end of 5 minutes after the start of the plasma as Δ_{LLS} -the powder signal, and that is plotted in the following figures.

4.3. Background

There are two schools of thought on powder formation in amorphous silicon deposition plasmas: One [1] suggests that powder is formed by reaction of reactive radicals with silane and higher silanes:

$$\begin{aligned} &SiH_2+SiH_4=Si_2H_6 \\ &SiH_2+Si_2H_6=Si_3H_8 \\ &SiH_2+Si_3H_8=Si_4H_{10} \quad \text{and so on.} \end{aligned} \tag{1}$$

Similarly for germane:

$$\begin{aligned} &GeH_2+GeH_4=Ge_2H_6 \\ &GeH_2+Ge_2H_6=Ge_3H_8 \\ &GeH_2+Ge_3H_8=Ge_4H_{10} \quad \text{and so on.} \end{aligned} \tag{2}$$

The other [2] claims that the reactions are between charged versions of the same species – presumably, the increased cross sections due to charge overcoming the lower number density compared to neutrals. From steady state generation and loss rate equations we obtain:

$$[Si_nH_{2n+2}]=(k_n/k_{n-1}k_{n-2}\ldots k_1)(X/\{1/\tau_n+\Delta Tk_T\})[SiH_4] \tag{3}$$

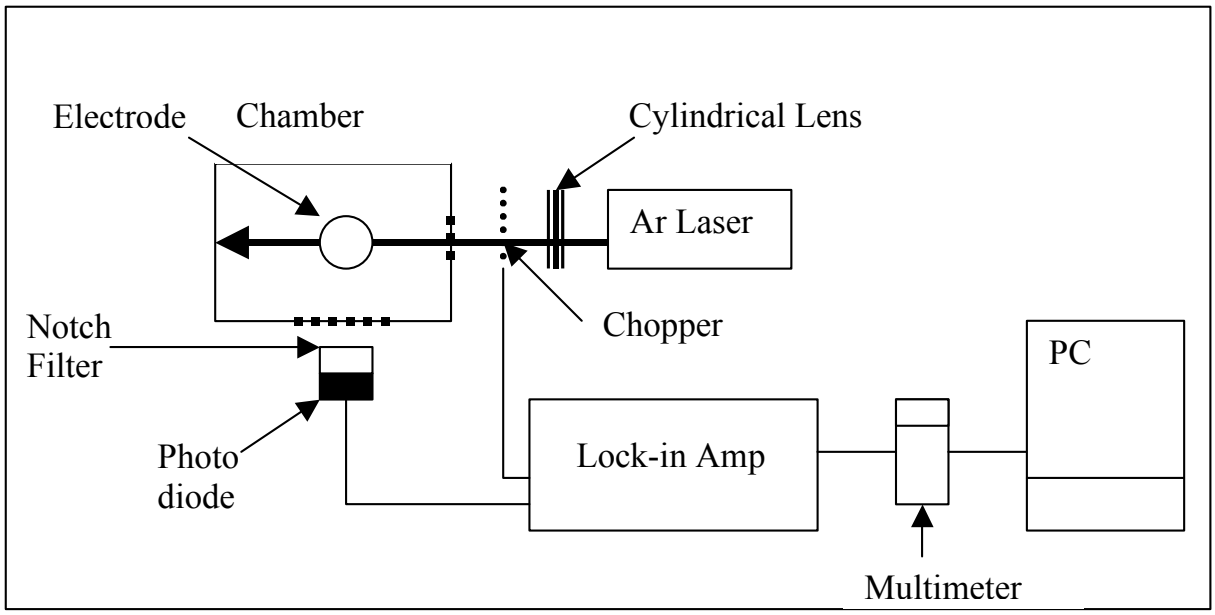

Figure 3. The schematic layout of the laser light scattering experiment.

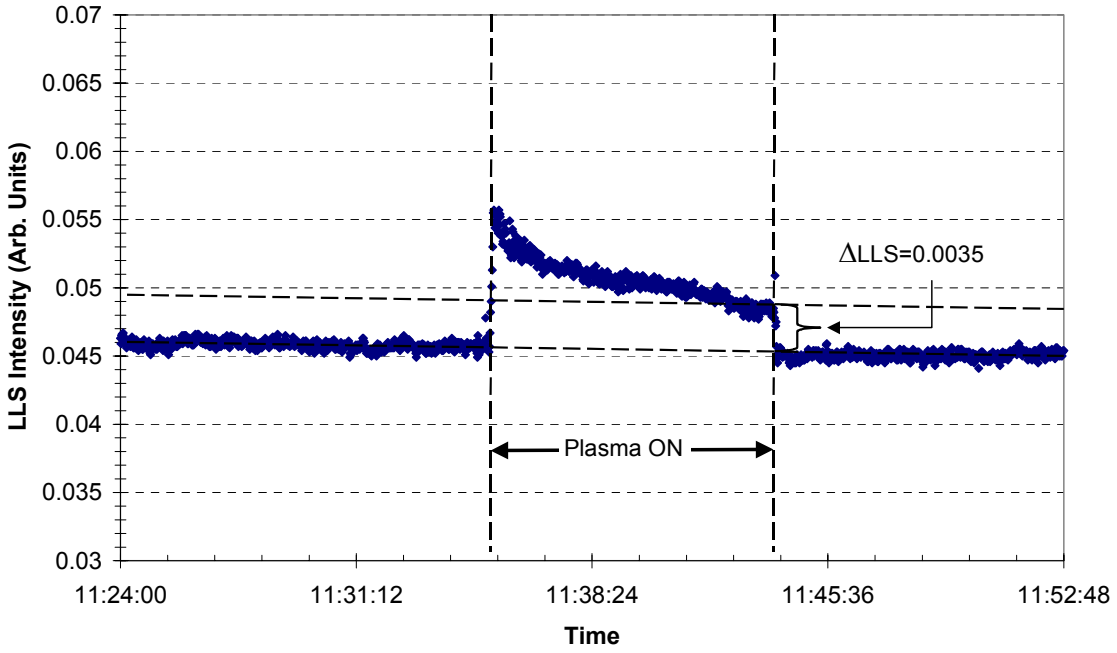

Figure 4. The laser-light scattering (LLS) intensity plotted as a function of time, before, during, and after a typical i-layer deposition.

which describes the steady state concentration rate of higher silane molecules. X contains the RF power dependence to power n. The temperature dependences of reactions 1 and 2 are in the reaction rate constants k. The thermophoretic force is $\Delta T k_T$ and the residence time is τ_n.

4.4. Influence of flow rate

Changing the flow rate alters the residence time of the gas and higher silane molecules. We can expect the residence time to depend weakly on the size of the molecules. Here we have plotted the scattering from powder as a function of the total flow rate keeping the dilution ratio and other conditions constant. Figure 5 includes points from experiments on different days all of which exhibit similar behavior. A similar figure has been plotted by Shiratani et al. [3]. The increase in the powder signal at the low flow rate side is due to the increasing partial pressure of silane ($[SiH_4]$ in eq. (3)) and the decrease at the high flow side is due to a decreased residence time (τ_n in eq. (3)). Because the higher silane molecules are supposed to affect the material quality and the cell performance, especially the stability, we are making a-Si:H solar cells with different total gas flow rates but keeping the dilution ratio the same. The solar cell performance and stability results will be presented in the future.

4.5. Effect of temperature

Both schools suggest that the reactions (1) and (2) are exothermic and therefore the density of powder decreases with increasing temperature [4]. This has been indirectly verified using the electron temperature - which decreases as the negative ions formed from powder particles decrease upon increasing the temperature [4]. The fact that these reactions are exothermic mean they have to be three body reactions and hence occur mainly at the electrode surfaces. Figure 6 shows the flow rate dependence as a function of temperature. We see that the effect from temperature depends on the actual flow rates used. From equation (3) we see that when the residence time term is short compared to the thermophoretic force term, the powder signal decreases with residence time (or increasing flow rates). At the lower flow rates, the complex dependence of the scattering intensity on flow rate and temperature is due to the interplay between the $k_n/k_{n-1}k_{n-2}\ldots k_1$, τ_n and $\Delta T k_T$.

In Fig. 7, we show similar data for a hydrogen diluted silane *plus germane* plasma. The behavior is seen to be similar. We also find that increasing the temperature reduces the powder as in the earlier figure for silane. There is a slight shift of the flow rate at the maximum powder point to higher flow. This is consistent with the observation that powder formation occurs more rapidly in germane relative to silane plasmas [5], and is investigated further below.

4.6. Effect of reactant gases

Next we have investigated the effect of replacing the silane flow with a fifth the flow of germane *assuming* that the decomposition rate of germane is 5 times that of silane. The hydrogen flow is kept constant so that the dilution increases and the residence time remains almost constant. Figure 6 shows (blue diamonds) that the powder related scattering goes through a minimum as we do this. The decrease is difficult to understand. It could be a consequence of the chemistry that silane related radicals do not react with germane and vice versa:

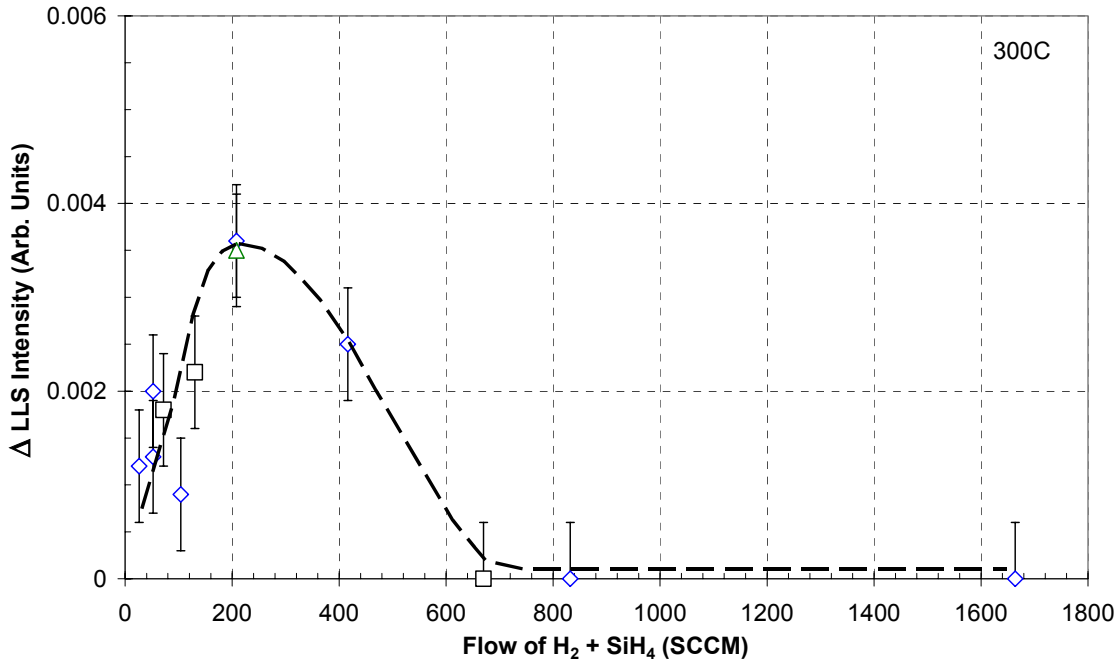

Figure 5. The laser light scattering intensity plotted as a function of the total flow rate at 300°C

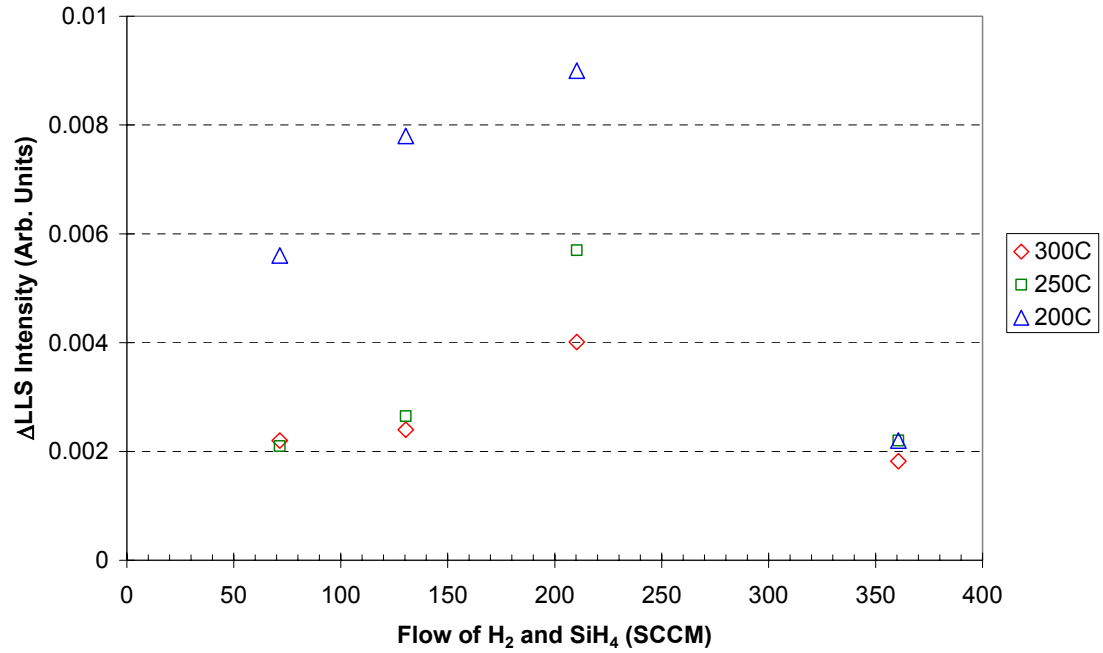

Figure 6. The laser light scattering intensity plotted as a function of the total gas flow rate at three different temperatures.

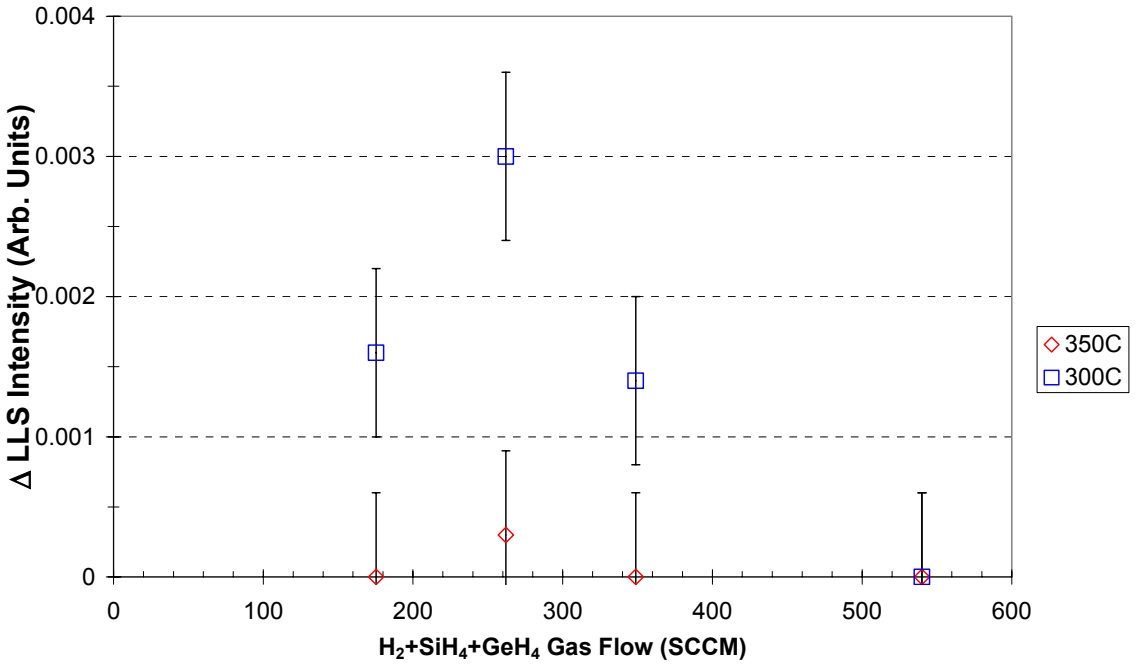

Figure 7. The laser light scattering intensity is plotted as a function of the total flow rate for silane plus germane gas mixtures at two different temperatures.

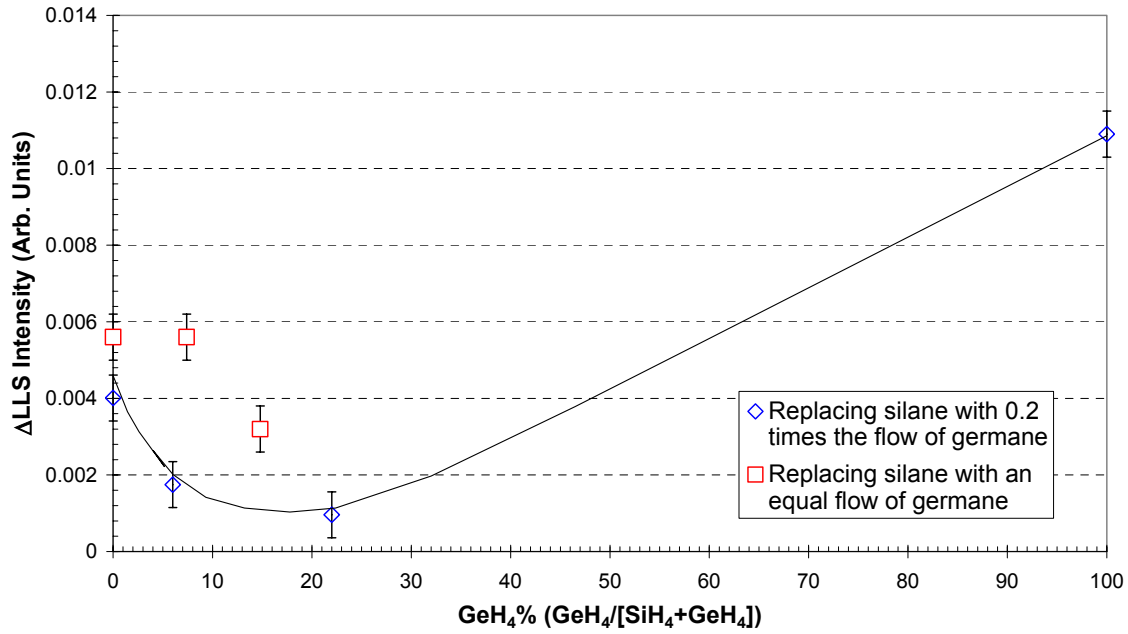

Figure 8. The laser light scattering intensity plotted as function of the germane to the total reactant gas ratio for two different ways of mixing the gases (see text)

SiH_2 + GeH4 $\Rightarrow$ No reaction
GeH_2 + SiH4 $\Rightarrow$ No reaction

Thus, as the germane partial pressure is increased, and the silane partial pressure decreased, the total reaction probability decreases. On the other hand, it could also be a consequence of the fact that the germane partial pressure increases by a fifth of the decrease of the silane partial pressure.

In order to examine this, we carried out a second experiment where we replaced silane flow with an equal flow of germane. This is shown by the red squares and we see that even in this case the powder-related scattering signal decreases. In this case, the hydrogen flow and dilution remain constant. Therefore, the decrease is likely due to the reduced reaction probability when the gases are intermixed. However, clearly the reactions between germane related radicals and molecules are faster than the silane related ones, and the scattering signal increases beyond about 20% germane to a higher value at germane 100% than at silane 100%. This is despite the higher hydrogen dilution at 100% germane by a factor of 5. We see that the chemistry of the plasma creates a 'sweet spot' where the total powder formation is lowest.

5. Effect of electrical bias on metastability in hydrogenated nanocrystalline silicon solar cells

5.1. Introduction

Light-induced defect generation in hydrogenated amorphous silicon (a-Si:H) based solar cells due to the Staebler-Wronski effect (SWE) [7] has been a subject of intense study. The light-induced defects reduce the mobility-lifetime product of the carriers, thus degrading solar cell performance. Hydrogenated nanocrystalline silicon (nc-Si:H), on the other hand, is reported to be stable against light soaking [8-10]. However, the best nc-Si:H cells are made near the transition from nanocrystalline to amorphous phase [11,12], where the nc-Si:H material contains a fraction of the amorphous phase. Klein *et al.* [13] reported that nc-Si:H cells near this transition made by the Hot Wire method show light-induced degradation. The magnitude of degradation depends on the hydrogen dilution ratio, and therefore, on the amorphous volume fraction. nc-Si:H cells made in our laboratory typically contain 40 – 80 % of crystalline volume fraction based on Raman spectroscopy [14]. These cells exhibit 3 to 15 % degradation under one sun white light illumination. However, these cells show no degradation when illuminated by red light with photon energies smaller than the bandgap of the amorphous phase [15], which indicates that defect generation in the amorphous phase causes the light-induced degradation of the nc-Si:H cells.

Metastable degradation in a-Si:H solar cells can also occur when the cells are subjected to prolonged forward bias [16,17]. In this case, double-carrier injection from the doped layers causes carrier recombination in the cell, which in turn creates metastable defects. On the other hand, applying a reverse bias to an a-Si:H cell during light soaking suppresses or eliminates the light-induced degradation by reducing the recombination of photogenerated carriers [18-20].

In this report, we present on the metastability of nc-Si:H solar cells by applying a forward bias in the dark, and a reverse bias on the cells during light soaking. Surprisingly, we find no forward current-induced degradation in the dark, but an enhanced light-induced degradation under reversed bias condition.

5.2. Experimental

Single-junction 1-μm thick nc-Si:H and 0.2-μm thick a-Si:H *nip* solar cells were deposited on 4 cm × 4 cm Ag/ZnO back reflector (BR) coated stainless steel (SS) substrates and specular SS substrates, respectively. The intrinsic layers were deposited using a modified very high frequency glow discharge method using a silane-hydrogen mixture at deposition rates ~ 3-8 Å/s. The solar cells were completed with indium-tin-oxide dots having an active-area of 0.25 cm^2 on the top *p* layer. Current density versus voltage, J-V, characteristics were measured in the dark and under an AM1.5 solar simulator at 25^oC. Light soaking experiments were carried out using 100 mW/cm^2 of white light at 25^oC and 50^oC under open-circuit condition or under an electrical bias. The forward double-carrier injection experiment was carried out in the dark at room temperature. For comparison, each experiment included both a-Si:H and nc-Si:H cells. The samples were annealed in vacuum at 150^oC for 2 hours before and after light/current soaking.

5.3. Results and Discussion

To check whether a forward double-injection causes degradation in the nc-Si:H solar cells, we applied a 1 V forward bias to the a-Si:H and nc-Si:H cells in the dark at room temperature. The initial forward current density was about 60 mA/cm^2 for the nc-Si:H cell and 3 mA/cm^2 for the a-Si:H cell. The temperature of the samples was monitored using a thermal-couple on the sample surface. No noticeable temperature increase was observed during the forward current injection. The kinetics of the FF under the forward bias are plotted in Fig. 9. One can see that the FF of the a-Si:H cell degrades continuously during the experiment time. This is simply due to new defects, generated by the recombination of excess carriers injected by the applied forward bias, which deteriorate the cell performance. The nc-Si:H cell, on the other hand, shows no degradation in the FF although the forward current density was much higher than that in the a-Si:H cell. The experiment has been repeated many times for different nc-Si:H cells and under different bias conditions. Table III summarizes the current-soaking data of open-circuit voltage (V_{oc}) and FF for one a-Si:H and three nc-Si:H cells. For the a-Si:H cell, V_{oc} decreased by 20 mV and FF by 5 % for a 1 V forward bias after 20 hours of current soaking, even though the forward current density was only 3 mA/cm^2. For the nc-Si:H cells, however, no current-induced degradation was observed in both V_{oc} and FF for all three cells with one cell (cell 4) having been subjected to 58 mA/cm^2 forward-current injection for more than 60 hours.

Next, we present the results of our study showing the effect of electrical bias on light-induced degradation in both the a-Si:H and nc-Si:H solar cells. For each experiment, two cells having similar initial J-V characteristics on the same substrate were selected for light-soaking simultaneously. One cell served as a reference that is light-soaked under the open-circuit condition. A reverse bias was applied to the other cell during light soaking. We first confirmed that the two cells on the same substrate show the same degradation after light soaking under the same conditions. Thus, any difference in the degradation magnitude for the two cells can be attributed to the effect of the applied bias. The experiment was repeated many times, and the results are reproducible. Typical results are listed in Table IV. One notes that, for the a-Si:H

Table III. Behavior of V_{oc} and FF for an a-Si:H (cell 1) and three nc-Si:H (cells 2-4) cells under various forward bias conditions in the dark.

Sample	State	V_{oc} (V)	ΔV (mV)	FF	$\Delta FF/FF_{in.}$ (%)
a-Si:H	Initial	0.998		0.696	
Cell 1	20 hr, 1V, 3 mA/cm^2	0.978	-20	0.664	-4.6
nc-Si:H	Initial	0.469		0.575	
Cell 2	15 hr, 0.5V, 7 mA/cm^2	0.469	0	0.579	+0.7
	Initial	0.469		0.591	
Cell 3	15 hr, 1V, 58 mA/cm^2	0.470	1	0.588	-0.5
	Initial	0.472		0.587	
Cell 4	64 hr, 1V, 57 mA/cm^2	0.474	2	0.590	+0.5

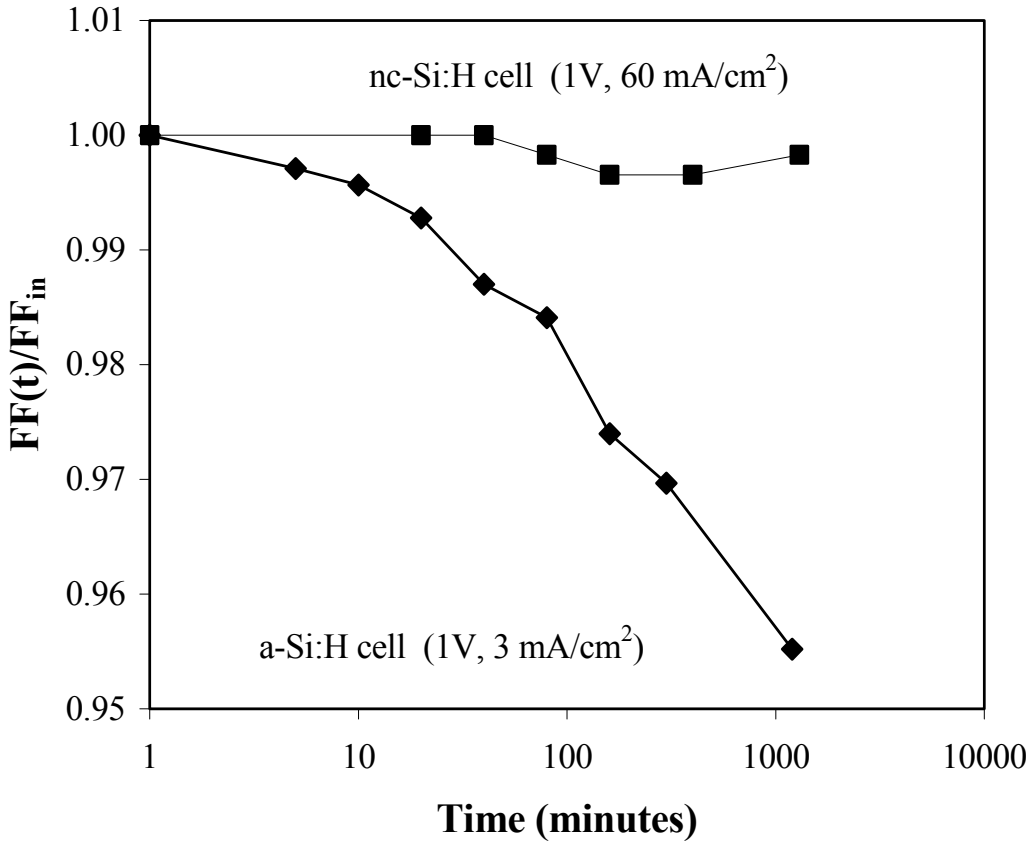

Figure 9. FF as a function of time, FF(t), normalized to the initial FF (FF_{in}) for an a-Si:H and a nc-Si:H single-junction solar cells with applied forward bias in the dark. The applied voltage and initial injected current densities are indicated.

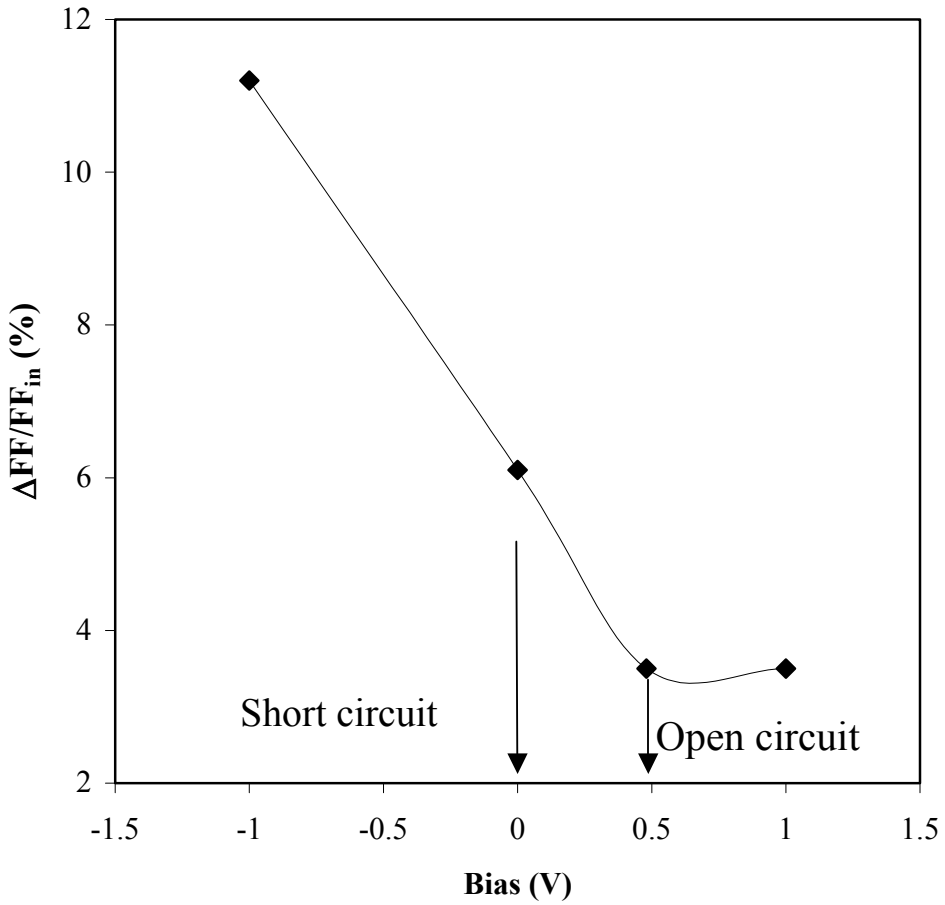

Figure 10. Light-induced degradation in FF of nc-Si:H solar cells versus the electrical bias during light soaking, where ΔFF denotes the variations in FF. Light soaking was carried out at 50^{o}C under one sun white light for 309 hours.

Table IV. V_{oc} and FF values for the a-Si:H (cells 1, 2) and nc-Si:H (cells 3, 4) cells before and after AM1.5 light soaking at 25°C with and without a –2 V bias.

Sample	State	V_{oc} (V)	ΔV (mV)	FF	$\Delta FF/FF_{in.}$ (%)
a-Si:H	Initial	0.984		0.695	
Cell 1	69 hr, no bias	0.954	-30	0.635	-8.6
	Initial	0.985		0.704	
Cell 2	69 hr, -2 V	0.983	-2	0.708	+0.6
nc-Si:H	Initial	0.476		0.591	
Cell 3	63 hr, no bias	0.467	-9	0.559	-5.4
	Initial	0.476		0.594	
Cell 4	63 hr, -2 V	0.427	-49	0.523	-12.0

cell under open-circuit conditions (cell 1), 69 hours of light soaking causes a decrease of 30 mV in V_{oc} and 8.6% in FF; while for the cell under a 2 V reverse bias (cell 2), there are no light-induced changes within the measurement uncertainty. The reduced/eliminated light-induced degradation by a reverse bias in the a-Si:H cell is commonly explained by the reduced recombination rate due to the enhancement of the internal electric field, which separates the electron-hole pairs more effectively. In contrast, the reverse bias effect on the light-induced degradation in the nc-Si:H cells is quite different from that in the a-Si:H cell. As shown in Table II, the V_{oc} of the biased cell (cell 4) decreased by 49 mV after 63 hours of light soaking, while that of the cell under open-circuit conditions (cell 3) decreased by only 9 mV. Similarly, the FF shows more degradation in the cell with applied reverse bias (12%) than under the open-circuit condition (5.4%). Apparently, a reverse bias in the nc-Si:H cell does not reduce but enhances the light-induced degradation. Figure 10 plots the degradation in FF versus the external bias. Short circuit is a zero bias condition, and open circuit is considered to be a forward bias condition with a bias value of V_{oc}. One can see that the light-induced degradation increases with the increase of the reverse bias voltage. However, a forward bias does not affect the light-induced degradation within the experimental uncertainty. In order to check whether the reverse bias causes any shunts in the nc-Si:H cells, we measured the dark J-V characteristics of the cell before and after light soaking. No shunt current is observed in either the annealed or light-soaked states. Instead, we observed an increase in the diode quality factor and the reverse saturated current density, indicating an enhanced recombination after light soaking.

We now discuss possible mechanisms for the observed phenomena. In general, nc-Si:H can be thought of as a mixed material comprised of nanocrystalline and amorphous phases. Thus, it is not difficult to understand the results of forward-current injection in the dark. The conductivity of the amorphous regions is much lower than that of the nanocrystalline regions. The forward injected current basically flows through the percolation path of nanocrystalline grains. We have shown previously that only the recombination events in the amorphous phase are responsible for the degradation in the nc-Si:H cell [15]. Since there are very few excess carriers injected into the amorphous phase, current induced degradation does not occur in nc-Si:H solar cells.

The reverse bias effect on the light-induced degradation in nc-Si:H is more difficult to explain, and we offer some conjectures. Our previous study showed that the recombination of photogenerated carriers in the amorphous and grain boundary regions is responsible for the light induced degradation of nc-Si:H solar cells [15]. The reverse-bias enhanced light-induced degradation in nc-Si:H solar cells implies that the recombination rate in the amorphous and grain boundary region is increased by the reverse bias during the light soaking. Microscopically, nc-Si:H is a two-phase material with nanocrystalline grains surrounded by amorphous tissues. Considering a given amorphous region, if both sides are nanocrystalline grains with a low bandgap, the interface region (grain boundary) between the amorphous and grains can form a microscopic diode. Along the current flow direction, an amorphous region is equivalent to two microscopic back-to-back connected diodes. These back-to-back diodes prevent current flows through the amorphous regions in the dark and no forward current-induced degradation is expected in the nc-Si:H solar cells. When the nc-Si:H cells are exposed to white light, excess carriers are generated in both the amorphous and nanocrystalline phases. The photogenerated carriers in the amorphous phase would transport through the nanocrystalline percolation path, and then to the doped layers. Before they can successfully leave the amorphous phase, they will recombine and generate defects. At the same time, the carriers generated in the nanocrystalline regions could also transport through the amorphous regions. The light-induced defects in the amorphous phase, especially in the grain boundary region, act as new recombination centers or traps that cause degradation in the solar cell performance. Even in a nanocrystalline path, the grain sizes are smaller than the cell thickness. One may think that elongated grains can exist throughout the entire 1 μm of thickness due to the columnar growth of the grain. However, AFM and TEM pictures showed fine structures inside larger grains [21,22], and XRD measurement revealed that the grain sizes are on the order of tens of a nanometer [9]. Therefore, even along a nanocrystalline path, carriers still need to pass many grain boundaries through the intrinsic layer, where light-induced defects could be generated. The metastable defects generated in the grain boundaries affects not only the cell performance but also the dark *J-V* characteristics.

When a reverse bias is applied to the cell, one of the diodes in the back-to-back diode configuration will be forward biased and the other reverse-biased. An external reverse bias will increase the electric field in the reverse biased region and cause a substantial drop in the field in the forward-biased region. Consequently, the forward-biased region will suffer enhanced degradation. For an applied forward bias, on the other hand, the external bias mainly drops in the *p/i* interface region due to the build-up of space charge. The intrinsic layer experiences a low field similar to the open circuit condition. The degradation will, therefore, not change very much.

In summary, we find that the effect of electrical bias on the metastability in the nc-Si:H cells is different from that in a-Si:H cells. Double-carrier injection under a forward bias in the dark does not result in any degradation in the nc-Si:H solar cell performance, but does cause a large degradation in the a-Si:H cell performance. We believe that the main transport path for forward injection carriers is through the nanocrystalline phase, where the recombination of carriers does not produce defects. On the other hand, applying a reverse bias during light soaking substantially enhances the light-induced degradation in the nc-Si:H solar cells, but suppresses the light-induced degradation in the a-Si:H solar cells. A possible explanation is presented on the basis of non-uniform field distribution in the heterogeneous material.

References:

[1] P.A. Longeway, Semiconductors and Semimetals (Academic Press, San Diego, 1984); M. Shiratani, S. Matsuo, and Y. Watanabe, Jpn. J. Appl. Phys. **30**, 1887 (1991).

[2] A.A. Howling, J-L. Dorier, Ch. Hollenstein, Appl. Phys. Lett. **62**, 1341 (1993); J. Perrin, A. Lloret, G. de Rosney, and J.P.M. Schmitt, Intl. J. Mass. Spec. Ion Process **57** 249 (1984).

[3] M. Shiratani, T. Fukuzawa, and Y. Watanabe. Jpn. J. Appl. Phys. **38**, 4556 (1999).

[4] A. Bouchoule, A. Plain, L. Boufendi, J. Ph. Blondeau, and C. Laure, J. Appl. Phys. **70**, 1991 (1991).

[5] S. Yokoyama, M. Tanaka, T. Yamaoka, M. Veda, and A. Matsuda, Proc. 5th Plasma Proc. Symp. (Nagoya 1988) p. 219; M. Takai, T. Nishimoto, M. Kondo, and A. Matsuda, Appl. Phys. Lett. **77**, 2828 (2000).

[6] H. Kawasaki, J. Kida, K. Sakamoto, T. Fukuzawa, M. Shiratani, and Y. Watanabe, J. Appl. Phys. **83**, 5665 (1998).

[7] D. L. Staebler and C. R. Wronski, Appl. Phys. Lett. **31**, 292 (1977).

[8] J. Meier, R. Flückiger, H. Keppner, and A. Shah, Appl. Phys. Lett. **65,** 860 (1994).

[9] J. Meier, P. Torres, R. Platz, S. Dubail, U. Kroll, J. A. A. Selvan, N. Pellaton-Vaucher, C. Hof, D. Fischer, H. Keppner, A. Shah, K.-D. Ufert, P. Giannoulès, and J. Köehler, Mater. Res. Soc. Symp. Proc. **420**, 3 (1996).

[10] K. Yamamoto, IEEE Transactions on Electron Devices **46**, 2041 (1999).

[11] O. Vetterl, F. Finger, R. Carius, P. Hapke, L. Houben, O. Kluth, A. Lambertz, A. Mück, B. Rech, and H. Wagner, Solar Energy Materials & Solar Cells **62**, 97 (2000).

[12] T. Roschek, T. Repmann, J. Müller, B. Rech, and H. Wagner, *Proc. of 28th IEEE Photovoltaic Specialists Conference* (IEEE, Anchorage AK, 2000), p. 150.

[13] S. Klein, F. Finger, R. Carius, T. Dylla, B. Rech, M. Grimm, L. Houben, and M. Stutzmann, Thin Solid Films **430**, 202 (2003).

[14] K. Wang, A. Canning, J.R.Weinberg-Wolf, E.C.T. Harley, and D. Han, Mater. Res. Soc. Symp. Proc. **808**, A9.53.1(2004).

[15] B. Yan, G. Yue, J.M. Owens, J. Yang, and S. Guha, Appl. Phys. Lett. **85**, 1925 (2004).

[16] R. A. Street, Appl. Phys. Lett. **59**, 1084 (1991).

[17] K. J. B. M. Nieuwesteeg, J. Boogaard, and G. Oversluizen, Mater. Res. Soc. Symp. Proc. **258**, 479 (1992).

[18] D. L. Staebler, R. S. Crandall, R. Williams, *Proc. of 15th IEEE Photovoltaic Specialists Conference*, (IEEE, Kissimmee, Florida, 1981), p. 249.

[19] L. Yang, L. Chen, J. Y. Hou, and Y. M. Li, Mater. Res. Soc. Symp. Proc. **258** 365 (1992).

[20] J. Yang, K. Lord, B. Yan, A. Banerjee, and S. Guha, *Proc. of 29th IEEE Photovoltaic Specialists Conference*, (IEEE, New Orleans, Louisiana, 2002), p.1094.

[21] E. Vallat-Sauvain, U. Kroll, J. Meier, and A. Shah, J. Appl. Phys. **87**, 3137 (2000).

[22] J. Kočka, A. Fejfar, H. Stuchlílová, J. Stuchlík, P. Fojtík, T. Mates B. Rezek, K. Luterová, V. Švrček, I. Pelant, Solar Energy Materials & Solar Cells **78**, 493 (2003).